Report submitted for the Astrophysics Laboratory 2 examination during the academic year 2021/2022 at University of Padova.

An Exoplanet Study: Revaluation of XO-2b

Akshay Kumar

Abstract

Using transiting and radial velocity observations modeled by a differential evolution Markov Chain Monte Carlo algorithm based to investigate the planetary system around the northern component of the XO-2 twin wide-binary system separated by $\sim$ 4500 AU. XO-2N is a solar-size K9V bright star have a super-solar metallicity (V = 11.18, [Fe/H] = 0.41), hosting a hot Jupiter XO-2b exoplanet with an orbital period 2.615856 ± 0.00006 days at 0.036779 ± 0.00014 AU, while having a radius $R_p = 0.998769 \pm 0.2379\, R_J$, mass $M_p = 0.596 \pm 0.009590\, M_J$. The transit solutions in good agreement with the reviewed literature, in fact, we enhanced the parameterization constraints on impact parameter and inclination.

1 Introduction

The first discovered planet orbiting outside the Solar system around a solar-type star was the hot Jupiter (a giant planet with a few days orbital period) 51 Pegasi by (Mayor & Queloz, 1995) using Radial Velocity (RV) observation. As of now, the number of the confirmed detected planets grew continuously to more than 4000 since the launching of space telescopes for transit detection, i.e., Kepler, TESS, most of them are hot Jupiter due to the biases toward short periods. However, only a small fraction of about 150 planets were observed in 102 binary systems, and 36 planets orbiting in 26 multi-star systems (complete list; univie). These numbers are significantly low considering the high frequency of binaries since the vast majority of the known planets orbiting a single star (Eggenberger et al. 2006; Marzari & Thebault, 2019), which may because of detection biases. Recently, a study of 290 planetary systems (Lea et al. 2020) concluded the planet's occurrence rate increase directly with stellar multiplicity, for instance, the occurrence rate around a wide-binary (i.e., XO-2 system) is 0.3 ± 0.04 planet-per-star compared with 0.12 ± 0.04 for a single star system, while about half of the formed planets in binaries were within 1 AU. The bright transiting S-type (orbiting only one of the binary's components) exoplanet orbiting the solar-size star XO-2N, known as XO-2Nb (XO-2b for short) considered a close-in giant, which is one of the extensively measured transiting exoplanets because of the system peculiarity. (Burke et al. 2007), first announced the discovery of a transiting planet around the metal rich star XO-2N of spectral type K0V in the wide-binary ($a_{bin} > 1000$) system XO-2, where the two components separated by a projected distance $a_{bin} \sim 4600$ AU. Accordingly, XO-2 is the seventh-widest binary hosting a planetary system. The southern star has its planetary system reported by astronomers from the Global Architecture of Planetary Systems program (GAPS) at Istituto Nazionale di astrofisica (INAF) in Padua (Desidera et al. 2014). This stellar-planetary system is unique as it is the first known binary system in which both stellar components have a planetary system. Despite that, the two stars are very similar even in their formation and evolution, they had given the birth of two very different planetary systems as the southern star XO-2S has two planetary companions, inner Saturn-mass XO-2Sb at 0.13 AU with eccentricity, e = 0.18 and outer Jupiter-mass XO-2Sc at 0.47 AU with e = 0.15 (Desidera et al. 2014), while the northern star XO-2N have one planet XO-2b at 0.036 AU in a circular orbit e = 0. The discovery paper of the exoplanet XO-2b (Burke et al. 2007) reported a Jupiter-size planet body with an orbital period, P $\sim$ 2.6 days, planetary radius, $R_p = 0.98 R_J$, and planetary mass, $M_p = 0.57 M_J$, a typical example of a Hot Jupiter class. In several studies devoted to investigating the atmosphere like (Pearson et al. 2019), the authors found XO-2b consistent with having a clear atmosphere. Clearly, expected from a close-in planet subjected to photoionization from the host star, with the existence of sodium and potassium lines, were both found in only a few Hot Jupiters. Spitzer space telescope IRAC performed secondary eclipse measurements (Machalek et al. 2009) which provide uncertain evidence for a weak temperature inversion in the upper atmosphere of the exoplanet as the day-side temperature $T_p \sim 1500K$, and modeled a substellar flux of 0.76×10^9 ergcm$^{-2}s^{-1}$, however, (Zellem et al. 2015), concluded to the host star XO-2N has an average variable activity of 0.0042 magnitude in R-band within 28.61 days, this variability essentially influence the transit observation and extracted parameters. Potentially, XO-2 system observed with different instruments in different bands such as Optical, Infrared, and Ultraviolet, in addition to multiple radial velocity observation. The system XO-2 is peculiar to study as there are 19 wide-binary systems hosting a planet(s) detected. However, only two systems were both stellar components have their own planetary system (S-type); WASP-94 (Neveu-VanMalle et al. 2014) and XO-2 (Damasso et al. 2015). The stars masses in these two particular systems $\sim 1 M_\odot$ as WASP-94 have 1.29 and 1.24 $M_\odot$ and XO-2 have 0.965 and 0.98 $M_\odot$, while the hosted planets have masses diverse between 0.259 and 1.37 M_J, with semi-major axes less than 1 AU. Moreover, HD-133131 system is also hosting planet for both of its component with separation of 360 AU.

2 Stellar parameters

The host XO-2N "Northern component" is a solar-size star with age $\sim$ 9 Gyr, Table 1A summarized the average stellar parameter values computed from the extensive previous works of the system, namely, Bonomo et al. 2017, Zellem et al. 2015, Crouzet et al. 2012, Southworth et al. 2012, Damasso et al. 2015, Baluev et al. 2015, Torres

et al. 2008. The star is relatively bright of magnitude: V=11.18±0.03, as obtained from Tycho-2 photometry (Hog et al. 2000, Burke et al. 2007). X0-2N and its companion have metallicity higher the most extra-solar systems known (Teske et al. 2013), 0.32 and 0.42. High metallicity systems have a higher probability of hosting planets (G. Mulders, 2018) and allowing large planetary core formation. Consequently, reaching the critical mass of gas accretion forming gaseous-giants nearby the host star (Benz et al. 2006). XO-2N and XO-2S nearly have the same stellar effective temperature with the difference $\Delta T_\star \sim 60$K, while magnitude difference is $\Delta R \sim 0.04$ and type that may be considered as early-type K (K0V) or late-type G stars (G9V). These similarities between these two twin stars provide an ideal comparison to study their planetary formation and evolution.

A. Stellar Parameters		
Effective Temperature (K)	$T_\star$	5320.5 ± 28.5
Metallicity (dex)	[Fe/H]	0.41 ± 0.021
Surface gravity (cms^{-2})	logg	4.418 ± 0.043
Parallax (mas)	θ	6.4539 ± 0.0603
Color magnitude	B − V	0.864 ± 0.03
Right Ascension	RA	07h48m06.47s
Declination	δ	+50d13m32.9s
B. Isochrone fit		
Mass ($M_\odot$)	$M_\star$	$0.965^{+0.011}_{-0.006}$
Radius ($R_\odot$)	$R_\star$	$1.02^{+0.009}_{-0.008}$
Density ($\rho_\odot$)	$\rho_\star$	$0.911^{+0.025}_{-0.023}$
Age (Gyr)	$t_\star$	$9.126^{+0.599}_{-0.913}$

Table 1: (A) Average values of the celestial coordinates and main stellar parameters of XO-2N estimated from the reviewed literature. (B) The Isochrone fit of stellar parameter computed from MESA/MAST project using PARAM interface website.

It is reported that XO-2N star showed evidence of variability based on the analysis of different instrument observations including 14 primary transit light curves in the photometric R-band (Damasso et al. 2015). Stellar main parameters needed for the analysis were computed using the website PARAM [1] (Da silva et al. 2006) using Bayesian estimation with posterior sampling performed by `MultiNest` introduced in Feroz & Hobson, 2008 , Feroz et al. 2009, Feroz et al. 2019, while the Modules for Experiments in Stellar Astrophysics (MESA) (Choi et al. 2016) Isochrones and Stellar Tracks (MIST) evolutionary models have been employed from A. Dotter, 2016 and Paxton et al. 2011 with spectroscopic parameters $T_\star$, [Fe/H], and logg listed in Table 1A, which are consistent with those in the SWEET-Cat catalog [2] show stellar observable parameters from the Isochrone fit within 1σ percentile as an estimate of the confidence interval in Table 1B. The limb darkening (LD) of the host star estimated using the quadratic expression; $I = 1 - c_1(1-\mu) - c_2(1-\mu)^2$, of two coefficients c_1 and c_2 from (A. Claret, 2018) and (Estaman et al. 2013). Considering fixed stellar atmospheric parameters of XO-2N, supported by a Monte Carlo approach employed with uniform distribution with sample size $N = 10^6$ to determine the influence of the uncertainty in T_* and logg on the estimation of LD coecients, considering 1σ percentile as an estimate of the confidence interval.

3 Observations

3.1 TESS observation

The Transiting Exoplanet Survey Satellite (TESS), launched in 2018. Approximately 200,000 bright main-sequence F, G, K, and M-type stars will be observed, searching for exoplanet candidates using the transit technique with enough precision to detect transiting planets smaller than Neptune ($R \leqslant 4R_\oplus$). TESS explores the sky in regions, each named Sector along the Northern, Southern, and ecliptic hemispheres. Each sector has a size of 2496 degrees. The target star XO-2N (TIC-356473034) observed during the period from December 25, 2019, to January 20, 2020, where XO-2 system appeared in CCD 1 of Camera 1 during sector 20 only. The target is considerably bright, observed at 2-minute cadence using an 1111 pixel subarray centered on the target, while the full-frame images (FFI) are collected every 30 minutes. FFI is the best public form of data provided by TESS collaboration which is a combination of science data and Collateral pixel data. The collateral data collected on-board to calibrate the actual science data and correct the biases, dark current, and charge smearing. Likewise, all the photometric data obtained by TESS pre-processed through Science Processing Operations Center (SPOC) pipeline (Jenkins et al. 2016) applied to the default optimal mask was chosen by the TESS/SPOC pipeline.

3.2 TASTE observation

The Asiago Search for Transit timing variations of Exoplanets (TASTE) described in (Nascimbeni et al. 2011), is a project that aims to detect Earth-like exoplanets using the Transit Time Variation (TTV) method, that enable the detection of planetary systems with relatively small masses using high precision imaging differential photometry with CCD of pixel size (0.26 arcsecond/pixel). A single light curve was obtained from Asiago observatory [3] on November 26, 2011 via 182 cm telescope. A total of 2999 data points were included without a pre-reduction as the TESS dataset, however, science frames are Raw data were treated manually using DS9 software (Joye & Mandel, 2003). The acquired dataset have three pieces; Science frames, Bias frames, and Flat-Field frames. The science frame must be reduced by correcting for the biases and Flat-Field effects; the Bias is an average count level added to the instrumental readout signal which not originate from the target and should be removed during the reduction process, the Flat-Field frames are used to calibrate the image by homogeneously illuminating the telescope pupil using a lamp illuminating a screen on the dome that used to measure the sensitivity of each individual pixel to normalize their response. Flat-field images must be corrected for bias, stacked together and, then nor-

[1] http://stev.oapd.inaf.it/cgi-bin/param
[2] http://sweetcat.iastro.pt/
[3] Based on observations collected at Copernico telescope (Italy) of the INAF - Osservatorio Astronomico di Padova

malized. Each frame reduced using master-bias and master-Flat frame, which linearly interpolated and applied for all frames.

3.3 Radial velocity observation

To acquire the mass and density of XO-2b exoplanet, the Radial Velocity (RV) observation obtained from two different instruments; the High-Resolution HARPS-N Spectrograph in the Canary Islands (Cosentino et al. 2012) at TNG in the framework of the GAPS programme, and the High-Resolution Spectrograph (HRS) on the McDonald Observatory which has one of the largest optical telescopes of size 11-m Hobby-Eberly Telescope (HET) (R. Tull, 1995). Table 2 provides the observation period, the Julian Date of the first spectrum obtained, and the number of spectra analyzed for each instrument. The HARPSN and HET data calibrated via Th-Ar simultaneous measurement to avoid stellar contaminant, then HARPS-N dataset reduced by the instrument pipeline and applying K5 mask then perform a weighted cross-correlation function. The RV data obtained from the available literature; HARPS-N dataset from table 7 in (Damasso et al. 2015) 2015, HET from table 3 in (Burke et al. 2007).

Instrument	Observation period (DD/MM/YY)	JD - 2450000 of 1^{st} observation	No. of spectra
HARPS-N	20/11/12 to 04/10/14	6252.7735	43
HET	27/01/07 to 01/03/07	4840.9616	30

Table 2: XO-2b Radial Velocity datasets used in this analysis.

4 Data reduction

4.1 TESS data reduction

Using `LightKurve` [4] package (Dotson et al. 2018) to search out Mikulski Archive for Space Telescopes (MAST) archive for the Target Pixel File (TPF) which is a raw form of data for a specific target, a cadence of the observed target produced every 2 minute. Each TPF is pre-processing using a defined adjustable mask that will use in the photometry. For the analysis presented in this report, we utilized the Simple Aperture Photometry (SAP). The presence of the unresolved binary companion could have a strong influence on the light curve if light entering the photometric aperture i.e. the mask, which causes a light curve dilution (Change the transit depth). This case is particularly relevant for TESS photometry because of its large pixel-size (21 arcsecond/pixel), since the angular separation between the Northern and Southern components of XO-2 is 31 arcsec. In order to do a careful analysis, likewise, we searched for TPF observation of our target binary companion XO-2S (TIC 356473029), then adjust the TPF mask manually shown in Figure 1b, by setting a threshold (quality selection) pixel's flux value to remove all background flux of sky and the contaminant star.

[4] https://github.com/KeplerGO/lightkurve
[5] https://github.com/jlillo/tpfplotter

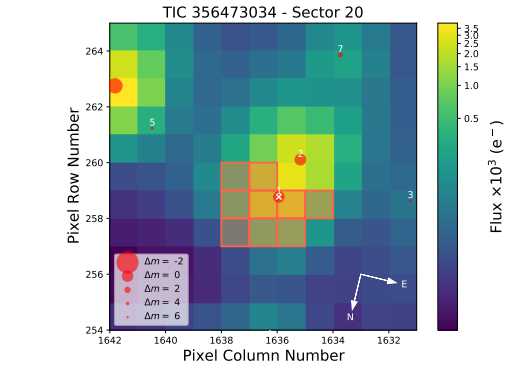

(a)

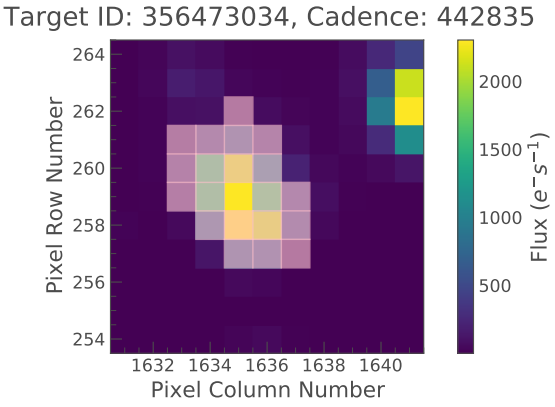

(b)

Figure 1: (a) Target Pixel File (TPF) of TIC-356473034 (XO-2N) plotted by tpfplotter, the red bordered pixels were used in the Simple Aperture Photometry (SAP), while the size of the red dots indicates the difference in TESS magnitudes of all nearby stars and the target XO-2N ($M_{TESS} = 10.4467$) that labelled with cross sign, as Label 2 indites the Southern component XO-2S.
(b) TPF CustomSAP mask covers the target and the contaminant companion star.

We used the default Simple Aperture Photometry pipeline which the pixel's flux obtained by subtracting the mean background count (bk) divided over it is the number of pixels (n_{bk}) multiplied by the total pixels (n) of the aperture from the mean pixel count $I = \sum_{ij} I_{ij} - n \times bk/n_{bk}$. Conventionally, we refer to the modified mask selected by custom Simple Aperture Photometry (CustomSAP). In Figure 1a. TPF was plotted with `tpfplotter` [5] (Aller et al. 2020) that shows the TESS magnitude difference Δm is between the contaminants and our target in the Gaia G-band (Gaia and the TESS photometric bands are very similar). The selected mask should contain contaminants of a difference $\Delta m < 2$, as shown that our target XO-2N and the contaminant star XO-2S have almost exactly the same TESS magnitude, thus $\Delta m = 0$. For the sake of comparison, another model used called Pre-search Data conditioning (PDC) when the SAP flux values normalized and corrected for instrumental fluctuations. This is the mission's best estimation of the intrinsic variability of the target (Osborn et al. 2020). Figure 2a. shows a comparison between the light curves obtained using FFI of size 20 pixels cutout, customSAP, SumSAP (computed from the sum of two SAPs procedures), and sumPDC (computed from the sum of two PDC-

SAPs), before eliminating points with anomalous flux using quality flag selection in the detrending process. From this point, we continue with CustomSAP photometry for the further analysis. Figure 2b, show the full TESS observation of target XO-2N flux treated using CustomSAP with no prior knowledge on neither the orbital period nor time of transit, even before the detrending process, the phase variation of planet's orbit is recognizable and easily see 9 distinguishable transits. The middle gap (contain an extra transit) of observation is due to the TESS satellite transition between two physical orbits within each sector (sector 20 in our case) where the telescope did not take any data during this time.

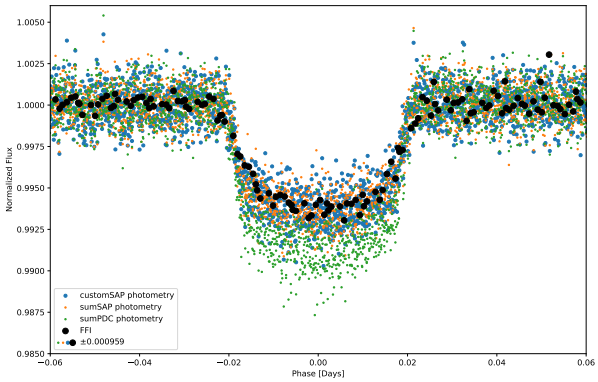

(a)

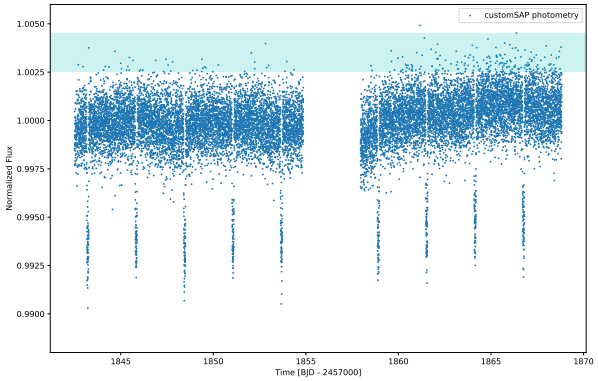

(b)

Figure 2: (a) The normalized folded light curve for XO-2b treated with different photometries; Simple Aperture Photometry (SAP), Pre-search Data Conditioned Simple Aperture Photometry (PDC), and a Full Frame Image (FFI). (b) The normalized flux before outlier-removed (detrend) when using Custom Simple Aperture Photometry (customSAP), outlier points donated by shaded cyan area. The gap in the middle of the sector time series separates the two physical orbits of the TESS spacecraft contained within the sector 20, the x-axis indicate the transit epoch.

The light curve detrending -flatten- by removing the instrumental and non-astrophysical source noise, and stellar activities or interruption trends within each pixel included in the mask. This procedure smooths the light curve by keeps the desired data for the planetary fit and increases the light curve precision without any distortion to the transit signal using a convolution-based function. The function `flatten` with biweight method from package `wotan` [6] (Hippke et al. 2019) were used with window length equal 1.00. The flattening process increases the light curve precision without any distortion to the transit signal using a convolution-based function. Figure 3a shows the folded flatten of the light curve around the planetary period after taking the mean CustomSAP flux with prior knowledge on the period P = 2.61585922 days and central transit time T_c = 2455565.546480 knowledge obtained from Damasso et al. 2015. However, the method of the first derivative of Huber's loss function (HUBER) `huberpsi` gave exactly the same result, but the biweight method adopted exhibit stronger signal detection efficiency (SDE) when fitting the produced light curve as will discuss next.

The Box Least Squares (BLS) (Kovács et al. 2002) is considered the standard algorithm tool searching out exoplanet transit, as it approximates the light curve into a box function and averages transit's flux to a fixed depth for the whole transit. BLS model is part of astropy [7] package which saves the computational power, and suitable for high signal-to-noise ratio (SNR) exoplanet signals i.e. Jupiter-like planets. For XO-2b, we used the BLS model to fit TESS data as get a period of P = 2.6155 days associated with signal-to-noise ratio, SNR = 149.3, and transit epoch Tc = 8843.2187. BLS detected 10 transits have maximum depth variation ΔFlux = 0.0057 with time series transit differ by 0.00003% from the following model (Figure 3). However, another approach considered by use Transit Least squares (TLS) Model adopted from package transit least squares [8] Hippke & Heller, 2019 with dependency on Bad-Ass Transit Model cAlculatioN (batman)[9] package L. Kreidberg, 2015. TLS detects transiting planets by using a transit-like function from time-series photometry, which more effcient to find any planet at even low SNR (unlike BLS) in the case of small planets. Most importantly, this algorithm is flexible to account for different Limb darkening coeffcients depend on user preference or other planetary effects that lead to approximate the light curve bottom to be more rounder than a fixed-line in the case of BLS. Using the quadratic LD expression, We found that c_1 = 0.4026 ± 0.018 and c_2 = 0.2012 ± 0.004 employed from A. Claret, 2018, which assumed to be fixed for the photometric band during the analysis. In contrast, A. Claret, 2017 model was used, the coefficients computed c_1 = 0.3879 ± 0.016 and c_2 = 0.2133 ± 0.003 considering 1σ percentile and same sampling size. It is worthy to note that, for both models, the medians of c_1 at fixed metallicity and fixed gravity are 0.3867, and 0.3927 respectively, and for c_2 are 0.2348 at fixed metallicity, and 0.233 at fixed gravity. For XO-2b, same as BLS, a total of 10 transits identified in the time series: ['8843.22445', '8845.83898', '8848.45351', '8851.06804', '8853.68257', '8856.29710', '8858.91163', '8861.52616', '8864.14069', '8866.75522'], with a planetary period, P = 2.61453 days, which have a maximum depth variation ΔFlux = 0.0064. In comparison, when

[6] https://github.com/hippke/wotan
[7] https://github.com/astropy/astropy
[8] https://github.com/hippke/tls
[9] https://github.com/lkreidberg/batman

considering HUBER flattening method, we obtained the exact same period and time series transits, but with weaker Signal Detection Effciency (SDE) than biweight (SDE = 20.1175) method by 5%.

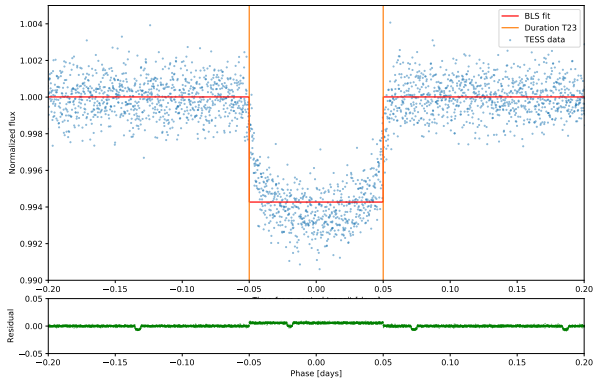

(a)

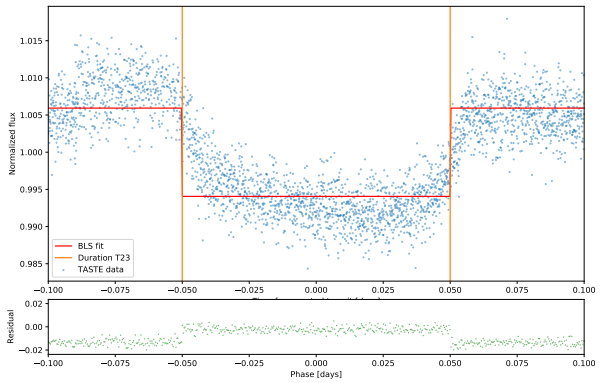

Figure 3: Box Least Squares (BLS) model fit for (a) TESS data. (b) TASTE data

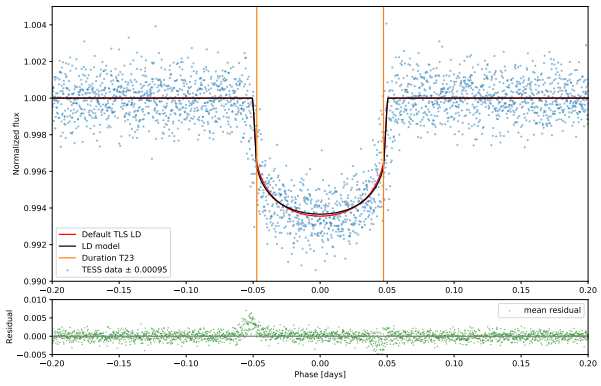

(a)

Figure 4: Binned light curve with TLS best-fit transit model for XO-2b exoplanet for both; default LD coeffcients searched by TLS algorithm (red) and this work LD coeffcients (black).

The TLS best-fit light curve shown in Figure 4 for the default limb darkening values searched by TLS algorithm from Mandel & Agol, 2002 LD model, similarly, for the TLS fit based on this work LD cofficient obtained before from A. Claret, 2018, the two models are well-matched, as the TLS with prior LD coefficients selection model shows a deeper transit which normalized flux at the center of transit equal 0.99366, which slightly higher than the TLS default model at 0.99356, we note to when LD coecients from EXOFAST model Estaman et al. 2013 tested which the same period and SDE, with a slight difference in transit depth, concluded at 0.99353. For the TESS analysis, TLS fit using A. Claret, 2018 LD model was favored.

4.2 TASTE data reduction

The first step of data reduction is using the differential photometry technique to obtain the magnitude measurements for the main target star and one (or more) reference stars, then the magnitude difference between them to determine the magnitude variation of the target to get the target's absolute magnitude (F_*); First, determine the differential photometric reference star (in our analysis HD 233451) which have the highest flux among the background stars, since Asiago Faint Object Spectrograph and Camera (AFOSC) having a field of view of 9090 that used to observe XO-2 system which is sufficientlywide to grant a precise selection. Secondly, select the appropriate aperture (the amount of light energy received per unit time) to measure the magnitude, by defining three annuli; inner annulus surrounding the target star, outer annulus include of double radius the inner one which have no contaminant star to define the sky background, and middle annulus separating the target and sky; then subtract the sky from the target's aperture, F_{apt} in green as $F_* = F_{apt} - F_{sky}$. This procedure cancels out the first-order systematic trends, for example, the atmospheric transparency variation. Once the absolute flux of the source is computed, combine the flux of reference star to be used as optimal reference flux for the photometry. In the pre-reduction procedures, we start by computing the master-bias frame, then use it to correct the Flat frame to produce the master-Flat frame, then use both master frames to correct the science raw frame to get a pre-reduced frame (.corr.fits). Next, use DS9 to apply differential photometry acquiring annulus dimension and radii, which used to construct the Point Spread Function (PSF) by setting a definite aperture radius that corrects the data into its final form that contains the flux for each aperture used. DS9 was used to compute PSF by selecting the target (XO-2N) and reference star from the pre-reduced frame at photometric aperture size R(68%, 90%, 95%, 99% of the Flux) avoiding any contaminant/nearby star (XO-2S). For our target XO-2N (V=11.18±0.03), apertures of size R(3pix) and R(6pix) correspond to 95%, and 99% respectively, were selected, with inner annulus radius a_{in} = 9pix and outer radius a_{out} = 17pix. After this selection, a Fortran-based code was performed on the selected aperture to extract light curve counts for all reduced science frames and for both apertures. Then, to normalize the flux, we divided the count of each aperture over the count-median of this aperture, also use correctly the time stamp to the Barycentric Julian Date in Barycentric Dynamical Time BJD_{TDB} as ;

$$\mathrm{BJD_{TDB}} = (2455892.432384 \pm 0.0002) + \mathrm{LT}$$

Where it is the sum Julian date at Earth barycenter for

the first science frame of observation, and LT which is the arrival time of photons at the heliocenter which obtained by creating a Sky-Coord object (the target Right Ascension and Declination) from astropy.time (Astropy Collaboration, 2013). A quality selection applied on data to eliminate outlier counts greater than the saturation level set that leads to 2905 points considered to the final orbital fit with flux less than 5.5×10^4 and greater than 80 for reference normalized flux (the absolute flux of the reference star normalized to 100 on the first frame) to eliminate airmass and atmosphere transparency issues. The produced light curve detrended as shown in Figure 3b, with the biweight filter then applied to BLS fit.

5 Discussion

5.1 Transit light curve solution

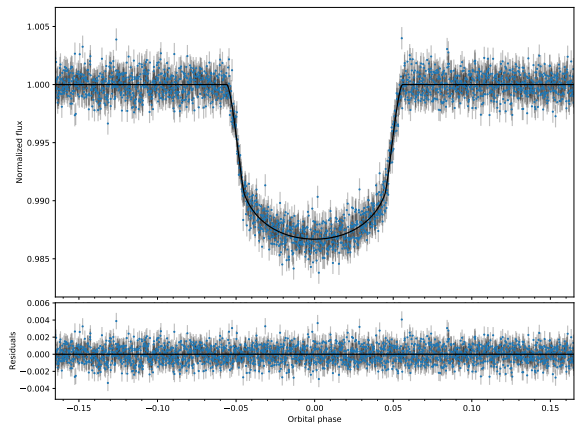

(a)

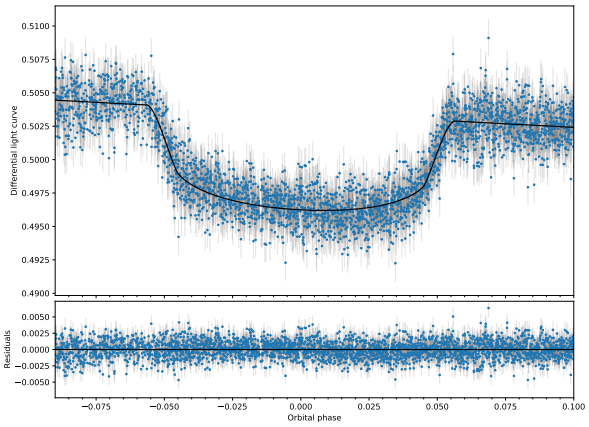

(b)

Figure 5: Light curve best-Fit using PyORBIT (a) TESS dataset, and (b) TASTE dataset

To characterize the planetary system parameters, a python-based package PyORBIT (Malavolta et al. 2016) was used to modeling the light curves obtained from TESS and TASTE, employing batman model (L. Kreidberg, 2015) of transit, as well as radial velocity spectra from HARPS, and HET. All priors were set uniformly in the linear space for a given parameter x from x - 0.05x to x + 0.05x, while some parameters adjusted to boundary values. The basic analysis done using compatible packages such as PyDE [10] (Storn & Price, 1997) which is a Global optimization solution using differential evolution to find the best global solution to the sampler package emcee11 to initialize the aneinvariant12 for Markov Chain Monte Carlo (MCMC) sampler (Goodman & Weare, 2010;(Foreman-Mackey et al. 2013), this combination used when the minimum or maximum of the function is not sufficient For transit light curves, a circular orbit assumed as the physical parameters' estimation of XO-2b exoplanet i.e. radius, mass, or orbital period, are adopted from (Estaman et al. 2013) model that considers the central time of transit Tc is the main parameter of the fit. In practice, we tested multiple models to fit the light curves: without priors on the limb darkening coefficients c_1 and c_2 and with priors on both coefficient

In case of TESS photometric fitting run, the fitting model corrected by accounting for the possible effect of the dilution from the stellar companion (as in this case with XO-2S) that may produce wrong transit parameters as the dilution affect the transit depth and the proper estimation of radius, which produce lower results than expected. Hence, the dilution factor of XO-2N star estimated to be d = 1.028 ± 0.008 from the formula;

$$d = 10^{(-0.4(T_{2S}-T_{2N}))}$$

Where the TESS magnitude close to the R-band of both stars obtained from https://exofop.ipac.caltech.edu/tess/, namely, XO- 2N is $T_2N = 10.446 \pm 0.006$ and the contaminant XO-2S, $T_{2S} = 10.416 \pm 0.006$.

We accounted for the 120 seconds exposure time of TESS when modelling the transit. For each model we run the sampler emcee for 10^5 steps, we then applied a burning of $2x10^4$ steps and a thinning factor of 100. Model with LD prior on coefficients are disfavoured with respect to the model without priors which shown in Figure 5a. The no LD prior best-fit solution obtained listed in Table 3. Generally, We found that all the parameters are consistent across the models with slight difference except for impact parameter which has high variability among runs by varying up to $\sim 9.8\%$. However, the impact parameter values in literature are not fully confined, hence, the NASA archive of Exoplanets reported 3 values; 0.089, $0.28^{+0.03}_{-0.04}$, and $0{:}158^{+0.11}_{-0.08}$ (Baluev et al. 2015); (Crouzet et al. 2012) (Torres et al. 2008), respectively, as our TESS result consistent with the litrature reference value of match the (Crouzet et al. 2012) within the error limits of 7.8%. The same approach was employed for TASTE, an additional model polynomial-trend (A method used to detrend the out of transit trend using low-order polynomial then normalize this fit over the MCMC iteration step) added to detrend any unsolved scattering due to systematic or unknown random errors. Also, the Gaussian prior on orbital period modified to be the refined values obtained from TESS light curve fit. The LD coefficients estimated using the photometric R-band (The closest to TASTE band) from (Claret & Bloemen, 2011) employed in EXOFAST model (Estaman et al. 2013) via the website exofast/limbdark selecting XO-2b target and stellar parameters in Table 1, we got coefficients of $c_1 = 0.4849$ and $c_2 = 0.215$. Table 3 showing the obtained planetary parameters when no LD priors defined for the fit which performed using polynomial trend with co-

[10] https://github.com/hpparvi/PyDE

Source	T_c [BJD_{TDB}]	T_{41} [days]	P [days]	R_p [R_J]	a [AU]	$R_p/R_\star$	$a/R_\star$	b	i [degree]	K [ms^{-1}]	M_p [M_{M_J}]	ρ_p [gm/cm^3]
Torres et al. 2008	-	-	2.615857	0.9830 ± 0.02	0.03684	0.10395 ± 0.0009	$8.2^{+0.1}_{-0.2}$	$0.15^{+0.11}_{-0.08}$	$88.90^{+0.60}_{-0.75}$	85 ± 8	0.566 ± 0.05	0.74 ± 0.1
Crouzet et al. 2012	2454508.73829 ± 0.0001	$0.111^{+0.006}_{-0.007}$	2.6158617	0.9930 ± 0.01	0.0368	0.10304 ± 0.0003	7.986 ± 0.07	$0.28^{+0.03}_{-0.04}$	$88.01^{+0.3}_{-0.2}$	-	0.566 ± 0.02	0.715± 0.04
Southworth et al. 2012	-	-	2.615864	$0.984^{+0.04}_{-0.08}$	0.03616	-	$8.08^{+0.3}_{-0.1}$	-	88.8 ± 1.2	92.2 ± 1.7	$0.593^{+0.04}_{-0.07}$	$0.77^{+0.15}_{-0.06}$
Bonomo et al. 2017	2455565.546480 ± 0.00005	-	2.6158592	1.019 ± 0.03	0.03665	-	-	-	$87.96^{+0.42}_{-0.34}$	90.17 ± 0.82	0.595 ± 0.02	$0.69^{+0.07}_{-0.06}$
This work analysis												
TESS	2458843.218564 ± 0.0001	0.111 ± 0.001	2.615856 ± 0.00006	$0.998^{+0.05}_{-0.02}$	0.0367	0.105 ± 0.001	$8.15^{+0.1}_{-0.2}$	0.17 ± 0.1	$88.5^{+0.9}_{-1.1}$	-	-	-
TASTE	2455892.432384 ± 0.0002	0.114 ± 0.0009	2.615848 ± 0.00008	$1.03^{+0.03}_{-0.01}$	0.0367	0.106 ± 0.001	7.95 ± 0.1	0.15 ± 0.1	$88.9^{+0.7}_{-0.8}$	-	-	-
RV	-	-	-	-	0.036		-	-	-	89.5 ± 1.2	0.596 ± 0.009	0.79 ± 0.05

Table 3: Main parameters obtained from PyORBIT fit of light curves obtained form TESS, and TASTE, and RV spectroscopy of HARPS-N and HET telescope, for XO-2b exoplanet. Compared to the reported values from previous literature. list of parameters in order; Central transit, transit duration, orbital period, radius, semi-major axis, ratio of planet to star radius, ratio of semi-major axis to host star radius, impact parameter, inclination, RV semi-amplitude, mass, and density.

efficients p_1 = -0.016 ± 0.0005 and p_2 = 0.502 ± 0.00004. We accounted for the 5 seconds exposure time of TASTE observation when modelling the transit. For each model we run the sampler emcee for 2.5x10^5 steps, we then applied a burn-in of 3x10^4 steps and a thinning factor of 100. The best solution model obtained from no LD prior set shown in Figure 6, with main parameters listed in Table 3. Considering runs of LD with and without prior model, the result slightly differs, which for some values such as radius seem outlying the NASA archive reference value 13, however, it is matching the one from (Bonomo et al. 2017). Likewise, for inclination as (Torres et al. 2008) which reported i = $88.9+^{+0.6}_{-0.7}$ and worth to note that the impact parameter is perfectly match same reference (Torres et al. 2008).

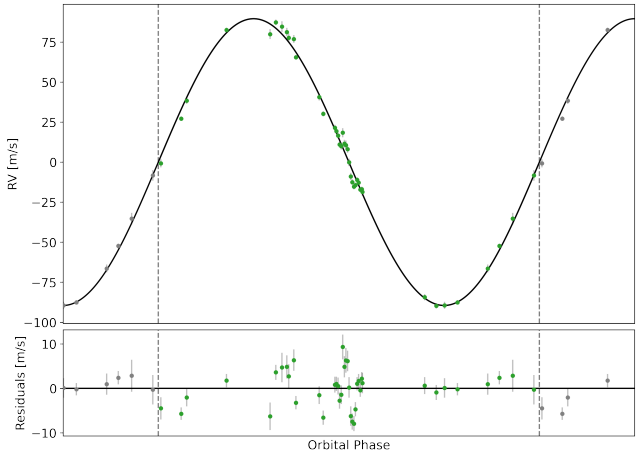

Figure 6: The radial velocity of XO-2N system obtained from HARPS-N + HET data which exhibit a sinusoidal oscillation with semi-amplitude, K = 89.539 ± 1.2 ms^{-1} .

The TASTE light curve shown in Figure 5b have a significant inclination, that may arise from the host star activity which also act as a contaminant which could add or remove flux depending on the activity configuration during the transit (Ioannidis et al. 2016). However, since the XO-2N have weak variability (Zellem et al. 2015), this inclination mostly caused by the airmass trend which is common in ground-based telescopes. During the differential photometry step, each star's flux changes with airmass at rate depending on the star's color (Blue stars extinct faster than red stars), since the only star in field-of-view was the chosen star, HD-233451 is more blue (B-V = 0.32) than the XO-2N (B-V = 0.86) which produce the expected tilt in the light curve (Gary, B. L. 2007).

5.2 Radial velocity results

We tested different data combinations and models with and without prior, using PyORBIT again with applying polynomial trend model of order 2, while optimizing priors based on photometric transits result obtained before as MCMC sampling ran with 10^5 steps. In practice, the best result obtained using the combined HARPS-N and HET datasets, with best-fit of polynomial-trend coeffcients 0.01, and -0.000006, giving a semi-amplitude of $K = 89.5 \pm 1.2$ ms^{-1} as shown in Figure 6. This model provided the best result; mass of $M_p = 0.596 \pm 0.009 M_J$, when used to estimate density with radius obtained from TESS data ρ_p = 0.79 gm/cm^3 while by using TASTE radius was $\rho_p = 0.71$ gm/cm^3. We got an independent estimation (without any priors) semimajor axis of 0.036 AU.

6 Summary

We extract the photometric light curves from the space-based telescope TESS and ground-based TASTE data, in addition to the radial velocity spectroscopy from HARPS-N and HET instrument. They observed the northern component of XO-2 wide-binary system during the period from January 27, 2007, to December 25, 2019. XO-2 hosting two similar G9V or K0V solar-size stars which the northern component XO-2N of magnitude V = 11.18 ± 0.03, hosting the exoplanet XO-2b. A Python-based PyORBIT program was used to search for the planetary parameter solutions for the transit light curves and radial velocity spectra using the emcee package employing Markov Chain Monte Carlo sampling in dependency on the PyDE package to find the global solution. The planetary parameters of XO-2b were extracted using uniform Gaussian priors in the linear space with the orbital period as a free parameter obtained from the Transit least squares model performed on TESS light curve using A. Claret, 2018 LD model. We present the following conclusions compared to the literature (Table 3):

- XO-2N have a super-solar metallicity, [Fe/H] = 0.41, with stellar parameters derived from the isochrone fit as; mass, $M_* = 0.965 \pm 0.011 M_\odot$, and radius, $R_* = 1.020 \pm 0.009 R_\odot$;
- XO-2b is a close-in gaseous giant planet of density, $\rho_p = 0.79 \pm 0.05$ gcm^{-3} estimated from mass, M_p = 0.596 $\pm 0.009 M_J$, obtained from RV spectra have semi-amplitude of $K = 89.5 \pm 1.2$ ms^{-1}, and radius, $R_p = 0.99 \pm 0.05 R_J$

References

[1] Duquennoy, A.; Mayor, M, Astronomy and Astrophysics, Vol. 500, p. 337-376 (1991/2009).

[2] Mayor, Michel; Queloz, Didier, Nature, Volume 378, Issue 6555, pp. 355-359 (1995).

[3] A. Eggenberger et al., Astronomy and Astrophysics, Volume 447, Issue 3, March I 2006, pp.1159-1163 (2006).

[4] Marzari, Francesco; Thebault, Philippe., Galaxies, vol. 7, issue 4, p. 84 (2019).

[5] Hirsch, Lea A. et al., eprint arXiv:2012.09190 (2020).

[6] C. Burke et al. The Astrophysical Journal, Volume 671, Issue 2, pp. 2115-2128 (2007).

[7] Desidera, S. et al., Astronomy & Astrophysics, Volume 567 (2014).

[8] Bonomo, A. et al., Astronomy & Astrophysics, Volume 602, id.A107, 16 pp. (2017).

[9] Zellem, Robert T. et al., The Astrophysical Journal, Volume 810, Issue 1, article id. 11, 9 pp. (2015).

[10] Crouzet, N. et al., The Astrophysical Journal, Volume 761, Issue 1, article id. 7, 13 pp. (2012).

[11] J. Southworth et al., Monthly Notices of the Royal Astronomical Society, Volume 426, Issue 2 (2012).

[12] J. Teske. et al., The Astrophysical Journal Letters, Volume 768, Issue 1, article id. L12, 6 pp. (2013).

[13] Mulders, Gijs D. Springer International Publishing AG, part of Springer Nature (2018).

[14] W. Benz et al., Direct Imaging of Exoplanets: Science Techniques. Proceedings of the IAU Colloquium (2006).

[15] M. Damasso et al., Astronomy & Astrophysics, Volume 575, id.A111, 24 pp. (2015).

[16] R. Baluev et al., Monthly Notices of the Royal Astronomical Society, Volume 450, Issue 3, p.3101-3113 (2015).

[17] G. Torres et al., The Astrophysical Journal, Volume 677, Issue 2, pp. 1324-1342 (2008).

[18] K. Pearson et al.,The Astronomical Journal, (2019).

[19] P. Machalek et al., The Astrophysical Journal, Volume 701, Issue 1, pp. 514-520 (2009).

[20] da Silva, L et al., Astronomy and Astrophysics, Volume 458, Issue 2, November I 2006, pp.609-623 (2006).

[21] E. Hog et al., Astronomy and Astrophysics, v.355, p.L27-L30 (2000)

[22] F. Feroz; M. P. Hobson., Monthly Notices of the Royal Astronomical Society, Volume 384, Issue 2 (2008).

[23] F. Feroz; et al., Monthly Notices of the Royal Astronomical Society, Volume 398, Issue 4 (2009).

[24] F. Feroz; et al., eprint arXiv:1908.04655 (2019).

[25] Choi, Jieun et al., The Astrophysical Journal, Volume 823, Issue 2, article id. 102, 48 pp. (2016).

[26] Dotter, Aaron., The Astrophysical Journal Supplement Series, Volume 222, Issue 1, article id. 8, 11 pp. (2016).

[27] B. Paxton et al., The Astrophysical Journal Supplement, Volume 192, Issue 1, article id. 3, 35 pp. (2011).

[28] Csizmadia, Sz et al., Astronomy & Astrophysics, Volume 549, id.A9, 11 pp (2013).

[29] Claret, Antonio., Astronomy & Astrophysics, Volume 618, id.A20, 4 pp. (2018).

[30] Claret, Antonio., Astronomy & Astrophysics, Volume 600, id.A30, 6 pp (2017).

[31] Claret, A.; Bloemen, S., Astronomy & Astrophysics, Volume 529, id.A75, 5 pp (2011).

[32] J. Eastman et al., Publications of the Astronomical Society of the Pacific, Volume 125, Issue 923, pp. 83 (2013).

[33] J. Jenkins et al., proceedings of the SPIE, Volume 9913, id. 99133E 20 pp. (2016).

[34] J. Dotson et al., Astrophysics Source Code Library, record ascl:1812.013 (2018).

[35] Aller, A. et al., S., Astronomy & Astrophysics, Volume 635, id.A128, 13 pp. (2020).

[36] HP, Osborn et al., Astronomy Astrophysics, Volume 633, id.A53. (2020).

[37] M. Hippke er al., The Astronomical Journal, Volume 158, Issue 4, article id. 143, 15 pp. (2019).

[38] Kovács, G.; Zucker, S.; Mazeh, T., Astronomy and Astrophysics, v.391, p.369-377 (2002)

[39] Hippke, Michael, Heller, René,. Astronomy & Astrophysics, Volume 623, id.A39, 13 pp (2019).

[40] L. Kreidberg, Publications of the Astronomical Society of the Pacific, Volume 127, Issue 957, pp. 1161 (2015).

[41] Mandel, Kaisey; Agol, Eric., The Astrophysical Journal, Volume 580 (2002)

[42] V. Nascimbeni et al., Astronomy & Astrophysics, Volume 527, id.A85, 10 pp. (2011).

[43] P. Kundurthy et al. The Astrophysical Journal, Volume 770, (2013).

[44] Sing et al., Astronomy Astrophysics, Volume 527, (2011)

[45] Joye, W. A., Mandel, E., Astronomical Data Analysis Software and Systems XII ASP Conference Series (2003).

[46] Astropy Collaboration, Astronomy Astrophysics, Volume 558, id.A33, (2013)

[47] Cosentino, R. et al., in SPIE Conference Series, Vol. 8446 (2012).

[48] Tull, R. G., Proc. SPIE, 3355, 387 (1995).

[49] J. Ge et al., Volume 7440, Techniques and Instrumentation for Detection of Exoplanets IV (2009).

[50] Malavolta, L et al., Astronomy & Astrophysics, Volume 588, id.A118, 12 pp (2016).

[51] Storn, R., Price, K., Journal of Global Optimization 11: 341–359, (1997).

[52] J. Goodman, J. Weare., Communications in Applied Mathematics and Computational Science, Vol. 5 (2010).

[53] D. Foreman-Mackey et al., Publications of the Astronomical Society of the Pacific, Volume 125 (2013).

[54] D. Kipping, Monthly Notices of the Royal Astronomical Society, Volume 435, Issue 3, p.2152-2160 (2013).

[55] Winn, Joshua N., eprint arXiv:1001.2010 arXiv:1001.2010.

[56] Steffen et al, Proceedings of the National Academy of Sciences, vol. 109, (2012).

[57] Latham et al., he Astrophysical Journal Letters, Volume 732, (2011).

[58] John Southworth., Monthly Notices of the Royal Astronomical Society, (2010).

[59] Seager, S.; Mallén-Ornelas, G., Scientific Frontiers in Research on Extrasolar Planets, Vol 294 (2003)

[60] J. M. Fernandez et al., The Astronomical Journal, Volume 137, Issue 6, pp. 4911-4916 (2009).

[61] M. Neveu-VanMalle et al., Astronomy Astrophysics, Volume 572, (2014).

[62] Ioannidis, P., Huber, K. F., and Schmitt, J. H. M. M., "How do starspots influence the transit timing variations of exoplanets? Simulations of individual and consecutive transits", Astronomy and Astrophysics, vol. 585, (2016)

[63] J. Teske et al., The Astronomical Journal, Volume 152, (2016).

[64] Gary, B. L., "Exoplanet Observing Tips", The Society for Astronomical Sciences 26th Annual Symposium on Telescope Science (2007)